Chemical Engineering Journal 502 (2024) 158099

Contents lists available at ScienceDirect

Chemical Engineering Journal

journal homepage: www.elsevier.com/locate/cej

Synthesis and characterization of eco-friendly cathodic electrodes incorporating nano Zero-Valent iron (NZVI) for the electro-fenton treatment of pharmaceutical wastewater

Dhiss Tesnim [a,b,**], Aida M. Díez [b,*], Hédi Ben Amor [a], M. Angeles Sanromán [b], Marta Pazos [b]

[a] National Engineers School of Gabes, Laboratory of Research: Processes, Energy, Environment & Electrical Systems PEESE (LR18ES34), University of Gabes, Republic of Tunisia

[b] CINTECX, Universidade de Vigo, BIOSUV Group, Department of Chemical Engineering, 36310 Vigo, Spain

ARTICLE INFO

Keywords:
Cathodic catalytic electrodes
Conversion of biomass
Green synthesis
Heterogeneous electro-Fenton
NZVI based materials
Pharmaceutical wastewater

ABSTRACT

The electro-Fenton process has the potential to be an efficient effluent treatment method, contingent on effective process optimization. It relies on two critical components: efficient in-situ H_2O_2 generation and the integration of highly reactive heterogeneous catalysts into electrode synthesis. In this study, several cathodic electrodes were synthesized, including those using zero-valent iron nanoparticles (P-NZVI), zero-valent iron nanoparticles supported on activated carbon (AC-NZVI), and El Hamma Bentonite clay loaded with zero-valent iron nanoparticles (HB-NZVI). These electrodes were fabricated using sustainable, straightforward methods and subjected to thorough physicochemical and electrochemical characterization. The goal of this research was to develop environmentally friendly cathodes, employing either pressed catalyst techniques or supporting the catalyst on carbon felt (CF) or titanium foil. These electrodes were evaluated within a heterogeneous electro-Fenton-like process, with a boron-doped diamond (BDD) anode, targeting the efficient degradation of the pharmaceutical pollutant Antipyrine (ATP). Among the tested configurations, the AC-NZVI/CF electrode demonstrated the highest degradation efficiency. Key experimental parameters, such as pH, current density, and water matrices, were systematically studied to optimize the process. Under optimal conditions (pH 7, current density of 55 mA A/cm^2), 80 % mineralization of a 40 mg/L ATP solution was achieved within 150 min, with an energy consumption of just 0.3502 kWh/g. The performance of the AC-NZVI/CF electrode remained stable when applied to real wastewater and after five consecutive cycles. Comprehensive analyses using FTIR, SEM-EDS, and XPS confirmed the stability and recyclability of the electrode, showcasing its potential for sustainable wastewater treatment applications.

1. Introduction

Among a variety of electrochemical-based advanced oxidation processes (EAOPs), the electro-Fenton process (EF) is acknowledged as a reliable and sustainably advantageous approach for the removal of persistent and hazardous pollutants that are oblivious to standard wastewater treatment techniques [1,2]. The heterogeneous EF presents distinct advantages over its homogeneous counterpart based on the electro generated H_2O_2 reaction with Fe^{2+} salts [3]. These include the ease of retrieving solid catalyst components, operating within a mild reaction environment across a broader pH range, and preventing the formation of iron sludge throughout the process [4].

As an alternative, the electro-Fenton-like process (EFL) employs transition metal catalysts, which interact similarly with H_2O_2 to initiate the oxidation reaction [3]. This H_2O_2 is *in-situ* generated via a two-electron oxygen reduction reaction (eq.1) occurring on the cathode. Subsequently, H_2O_2 is decomposed with a metal ion (M^{n+}), producing a $HO^{\bullet}$ radicals and a metal in an oxidized state (M^{n+m}) (eq.2), facilitating the degradation or complete mineralization of organic pollutants [5]. The effectiveness of EFL can be enhanced through both the anode and cathode electrodes. Indeed, the adsorption of $HO^{\bullet}$ radicals (eq.3) generated on the anode (M) surface by water oxidation plays a crucial

* Corresponding author.
** Corresponding author at: National Engineers School of Gabes, Laboratory of Research: Processes, Energy, Environment & Electrical Systems PEESE (LR18ES34), University of Gabes, Republic of Tunisia.
E-mail addresses: tesnim.dhiss@enig.rnu.tn (D. Tesnim), adiez@uvigo.gal (A.M. Díez).

https://doi.org/10.1016/j.cej.2024.158099
Received 11 August 2024; Received in revised form 23 November 2024; Accepted 26 November 2024
Available online 28 November 2024

role in this enhancement. Additionally, the cathode has a significant impact on the *in-situ* generation of H_2O_2, greatly influencing its subsequent catalytic reaction mechanism and kinetics [6]. An ideal cathode for this process should exhibit high stability, excellent mechanical strength, and a sufficiently large specific surface area. Moreover, it should be versatile enough to be adapted to various shapes and surfaces, all of this while exerting minimal to no influence on the subsequent catalytic decomposition of H_2O_2 [7].

$$O_2 + 2H^+ + 2e^- \rightarrow H_2O_2 \quad (1)$$

$$H_2O_2 + M^{n+} \rightarrow HO^{\bullet} + OH^- + M^{n+m} \quad (2)$$

$$H_2O + M \rightarrow M(HO^{\bullet}) + H^+ + e^- \quad (3)$$

In recent years, there has been growing interest in enhancing the performance and versatility of EFL by developing the synthesis of cathodes. These electrodes are designed not only to catalyse ELF reactions but also to facilitate the generation of H_2O_2, a crucial intermediate in the process [8].

Despite the established efficacy and stability of powder catalysts, contemporary research has shifted towards exploring novel electrode materials with tailored electrocatalytic properties [9]. Cathodic electrode fabrication integrates catalytic phases onto carbonaceous supports through methods like physical deposition, chemical modification, or electrodeposition [10]. The choice of the catalyst depends on EFL requirements and performance metrics [11]. Previous studies have investigated various catalysts, including transition metal nanoparticles such as zero-valent iron nanoparticles (NZVI) [12], metal–organic frameworks MOFs [13], clays [14] and carbonaceous materials [4] for their diverse activities and selectivity in fine-tuning the EFL for pollutant degradation. Green NZVI has garnered effective interest for use in EFL treatment due to its cost-effectiveness, accessibility, and potent reduction potential [2]. However, NZVI particles must contend with issues like passivation, quick agglomeration, and decreased reactivity over time [15]. In order to get beyond these restrictions, combining NZVI with supports materials like activated carbon [2], biochar [16], and clay [17] helps overcome these difficulties. In addition, carriers offer mechanical support, which prolongs NZVI's reactivity in aqueous environments and slows passivation [9,18].

Extensive research has been conducted on various cathode materials to enhance the efficiency of the EFL. Among these, carbon-based materials have attracted considerable attention due to their exceptional electrochemical properties. Materials such as graphene felt [14], carbon felt (CF) [19], activated carbon (AC) [20] and carbon black (CB) [21] are particularly valued for their high electrical conductivity, availability, cost-effectiveness, and sustainability. These qualities make them ideal candidates as conductive supports in cathodes, further improving the overall performance of the process [22]. In the manufacture of a cathode, a binder is crucial for forming bonds that hold the active substances in place. This enhances the contact between the electrode's active material and the conductive agent, thereby establishing a continuous conductive network throughout the electrode [23]. The use of polyvinylidene difluoride (PVDF) as a binder is favoured due to its exceptional adhesion properties and electrochemical stability [24]. In other studies, polytetrafluoroethylene (PTFE) was used as a cathode binder, improving the capacity, low cost and the generation rates of H_2O_2 [25].

Despite these advancements, significant gaps remain, particularly in the long-term stability of NZVI-based electrodes in the EFL process [18,26]. Many catalysts face rapid deactivation due to iron passivation or electrode fouling, limiting their effectiveness over extended operational periods [27]. This study seeks to address these challenges by developing an eco-friendly cathodic electrode incorporating NZVI, supported on abundant natural, low-cost materials. By enhancing the catalytic activity and stability of the NZVI-based cathode, this work aims to advance the sustainability and scalability of the EFL process for large-scale wastewater treatment.

A key focus of electrode modification in EFL systems is to increase the yield *of in-situ* H_2O_2 generation while incorporating highly reactive heterogeneous catalysts into the cathode to boost HO• radical production through the Fenton reaction. The novelty of this work lies in synthesizing cathodes using three different methods, all utilizing abundant, low-cost, and environmentally friendly catalysts. Firstly, it was utilized PTFE and CB to enhance the *in-situ* H_2O_2 yield, while incorporating heterogeneous catalysts including P-NZVI, or its combination with AC or HB so-called AC-NZVI, and HB-NZVI into CF-based of Ti-foil composite cathodes. Secondly, a hand-pressed method, blending PTFE, CB, and the catalyst materials (AC-NZVI, P-NZVI, and HB-NZVI) was employed.

The morphology, surface characteristics, and electrochemical properties of these cathodes were comprehensively examined. Simultaneously, employing ATP as the target pollutant, the potential and performance of the composite electrode as the cathode of the EFL were evaluated. This assessment encompassed the cathode's ability to produce and activate H_2O_2 *in-situ*, its stability, reusability, and its efficiency in degrading ATP. Synthetic drugs, exemplified by ATP, have been extensively employed to uphold human health as antipyretics and analgesics have been detected in numerous aquatic settings [9]. However, the excessive release of these synthetic compounds has led to widespread water contamination, posing significant environmental challenges and jeopardizing ecosystem equilibrium. This class of drugs fosters drug resistance in microorganisms and disrupts the growth and reproduction of aquatic organisms, exacerbating the situation. Due to its mutagenic and carcinogenic properties, ATP represents a hazardous organic pollutant that requires urgent removal from pharmaceutical wastewater [2]. This study proposes a novel and efficient alternative for ATP elimination thought EFL.

2. Experimental Section

2.1. Reagents

Carbon mesoporous nano-powder graphitized (so-called CB), PTFE (60 wt% H_2O), PVDF and 1,3-dipropanediol (NMP), sulphuric acid, sodium hydroxide , potassium titanium oxalate dehydrate and ATP were obtained from Sigma. The electrolyte sodium sulphate (Na_2SO_4) was purchased from ITW Reagents. All chemicals were of analytical grade. Carbon-Lorraine provided the CF RVG 2000, while Condias provided the BDD. Titanium foil (thickness of 0.03 mm), was purchased from Sigma-Aldrich.

The materials P-NZVI, AC-NZVI, and HB-NZVI have been synthesized and characterized in previous works [28,2] and [17], respectively.

2.2. Manufacturing of electrode

The preparation of electrodes was performed according to the methodologies proposed by Poza-Nogueiras et al. [20], Li et al. [14] and Del Álamo et al. [9], with some modifications to optimize reproducibility and material performance. Three different materials: P-NZVI, AC-NZVI, and HB-NZVI, referred to as M were used to synthetize the electrodes. The electrode formulation consistently comprised 85 wt% of the active M material powders, 10 wt% polymer binder (chosen based on compatibility and strength), and 5 wt% carbon black (CB) for conductivity enhancement. Each electrode was standardized to a volume of 4 cm^3 (2 cm × 2 cm × 1 cm) to ensure consistency in electrochemical performance across methods. The techniques and material specifications are summarized in Table S1.

Method A: Immobilization onto Carbon Felt (M/CF Electrode), was based on the procedure described by Li et al. [14], with steps tailored to achieve optimal adhesion and uniformity. The CF electrodes were sectioned into 2 cm × 2 cm pieces, cleaned by soaking in 100 °C nitric acid (HNO_3) for 2 h, followed by acetone washing and ultrasonic

cleaning with distilled water. This ensured the removal of impurities and enhancement of the surface area for better material bonding. The CF was dried at 105 °C for 12 h to further ensure surface stability. A slurry was prepared by combining 2.762 g of M, 0.162 g of CB, 250 μL of PTFE (binder), and 25 mL of deionized water. This mixture was sonicated for 30 min to ensure uniform dispersion of all components. The pre-treated CF was immersed in the slurry, and after achieving a uniform coating, the electrode was vacuum-dried at 80 °C for 24 h. This optimized procedure promotes strong adhesion of the catalytic layer, maximizing its activity during EFL testing.

Method B: Application onto Titanium Foil (M/Ti Electrode), was adapted from Poza-Nogueiras et al. [20], where the blend was applied to titanium foil (Ti). An ink was prepared by dispersing 0.977 g of M powder, 0.115 g of PVDF (binder), and 0.057 g of CB in 30 μL of N-methyl-2-pyrrolidone (NMP). This ink was then applied to both sides of the Ti foil using a precision coating process to ensure uniform coverage. The coated Ti foil was subsequently dried in a vacuum oven at 60 °C overnight. This method was chosen due to the superior conductivity and corrosion resistance of Ti, which significantly enhances the electrode's electrochemical stability, especially for repeated use in EFL experiments.

Method C: Hand-Pressing onto Composite Electrode (M Electrode), based on hand-pressing technique, adapted from Del Álamo et al.[9], to create an electrode composed primarily of CB and PTFE. A mixture was prepared by combining 0.1 g of CB, 5 mL of distilled water, and 200 μL of a PTFE solution (containing 60 wt% PTFE). Then, 2 g of M material was added to form a composite, and the mixture was hand-pressed into a flat-plate electrode. The electrode was then dried at 80 °C for 2 h to ensure proper bonding. This approach was selected for its simplicity and ability to produce an electrode with robust mechanical properties while maintaining good catalytic performance.

2.3. Physicochemical and electrochemical characterizations of composites electrodes

The composite electrodes synthesized were thoroughly characterized to examine their elemental composition and microstructure. Scanning Electron Microscopy and Energy Dispersive Spectrometry (SEM-EDS) were performed using a JEOL JSM6010LA equipped with an EDS Oxford Aztec One SEM (Oxford Instruments, England). This allowed for detailed examination of the materials' surface morphology and elemental composition. Chemical interactions within the materials were probed using FT-IR Nicolet 6700 infrared spectrometer (Thermo Fisher Scientific Inc., United States). X-ray diffraction (XRD) analysis was utilized to investigate the crystalline structure and phase purity of the samples. Elemental composition analysis was carried out using a Horiba Jobin Yvon HR800UV spectrometer and X-ray photoelectron spectroscopy (XPS). These measurements were performed at CACTI, University of Vigo (ESP).

Cyclic voltammetry (CV) was utilized to assess the electrochemical properties of the functional catalysts. A three-electrode cell setup was employed, comprising an Ag/AgCl reference electrode, a platinum wire (0.5 × 100 mm) as the counter electrode, and the functional electrode as the working electrode. The experiments were conducted using a potentiostat model PGSTAT302 N (Metrohm Autolab, The Netherlands). CV measurements were performed in a 100 mL solution of 1 M NaOH, with the potential scanned between 0 and 0.74 V. Additionally, Electrochemical Impedance Spectroscopy (EIS) measurements were carried out across a frequency range from 10^{-1} to 10^{6} Hz, with a voltage amplitude of 10 mV.

2.4. Heterogeneous EFL experiments

The prepared electrodes were employed in heterogeneous EFL experiments, conducted in a 150 mL undivided cylindrical electrochemical cell. The solution of 0.05 M Na_2SO_4 was employed as the supporting electrolyte, and the volume of the pollutant solution contained 40 mg/L of ATP was fixed at 100 mL. A two-electrode configuration was used, with the manufactured electrodes (2 × 2 cm) serving as the cathode and a boron-doped diamond (BDD) electrode as the anode. The electrodes were positioned 2 cm apart, ensuring optimal current distribution and efficiency. The electrochemical cell was continuously stirred at 400 rpm using a magnetic stir bar to ensure uniform mixing of the solution and to facilitate effective mass transfer during the reaction. The pH of the solution was initially adjusted to 3 using 0.5 M sulphuric acid, to enhance the generation of hydroxyl radicals and the EFL process, as commonly observed in electrochemical degradation studies. Air was continuously pumped into the solution at 1 L/min to provide additional oxygen for the reaction and maintain oxygen saturation, improving the overall catalytic performance. Before starting the electrochemical treatment, the electrodes were immersed in the solution and allowed to equilibrate for 30 min to measure any potential ATP adsorption onto the electrode surface. This pre-treatment phase ensured a stable baseline for assessing ATP degradation efficiency.

Every experiment was carried out twice, and the standard variation of the pharmaceutical pollutant content was found to be less than 5 %.

The specific energy consumption (EC) per mass unit of removed pollutant (ATP) was calculated using (Eq.4) [29]:

$$EC\left(\frac{kwh}{g}\right) = \frac{U^{*}I^{*}t}{\Delta C^{*}V} \tag{4}$$

where ΔC was the difference between the ATP concentration (mg/L) before and after the reaction, U was the applied cell voltage (V), I was the average current intensity (A), V was the solution volume (L) and t was the time (h).

2.5. Kinetic studies of ATP degradation

The degradation kinetics analysis was conducted to compare the degradation rates and elucidate the role of $HO^{\bullet}$ radicals. The $HO^{\bullet}$ radicals generated in the system (Eqs. (2) and (3) are crucial for the degradation of ATP and its intermediates.

To quantitatively describe the removal kinetic of ATP, zero-order (ZO), pseudo-first-order (PFO), and pseudo-second-order (PSO) models were applied to the experimental data, as shown in Eqs. (5) to (7), respectively:

$$C_t - C_0 = -k_{app0}t \tag{5}$$

$$ln\frac{C_0}{C_t} = -k_{app1}t \tag{6}$$

$$\frac{1}{C_t} - \frac{1}{C_0} = k_{app2}t \tag{7}$$

where C_0 represents the initial concentration of ATP, C_t represents the concentration of ATP at time t, k_{app0}(mg/L.min), k_{app1} (min^{-1}) and k_{app2} (L/mg.min) are the rate constants for ZO, PFO and PSO reactions, respectively.

2.6. Electrochemical assays on real wastewater

Under optimal conditions, electrochemical assays were performed using a real water matrix obtained from the effluent of the wastewater treatment plant situated in Guillarei (Spain). This matrix was doped with 40 mg/L of ATP. The real wastewater (RW) demonstrated a significant level of complexity, as depicted in Table 1. The abbreviations and full names of the parameters are provided in Table S2.

2.7. Analysis techniques

ATP concentration was measured using an Agilent 1100 HPLC

Table 1
Physicochemical parameters of the RW.

Parameters	DCO	SS	DBO_5	pH	C	N_{tot}	P_{tot}	NO_3^-	NH_4^+	NO_2^-
Values	37	7	2	7.1	239	7.66	0.55	6.38	0.17	0.002
Units	mg/L	mg/L	mg/L	–	µs/m	mg/L	mg/L	mg/L	mg/L	mg/L

equipped with a Zorbax Eclipse XDB C8 (150 mm × 4.6 mm, i.d., 5 µm) column (Agilent) with a DAD detector set at 243 nm (λ_{max}). As the mobile phase, a mixture of 1.5 % acetic acid and acetonitrile (10:90 v/v) was utilized at a flow rate of 1 mL/min.

The H_2O_2 concentration was determined using Sellers' titanium oxalate method [30] which yields a yellow-orange titanium (IV) peroxide complex in the presence of H_2O_2. The absorbance at 405 nm of this complex, proportional to H_2O_2 content, was measured using a GENESYS 150 UV–Vis Spectrophotometer (Thermo Fisher Scientific, Madrid, Spain).

Total Organic Carbon (TOC) was determined using a non-dispersive infrared detector (CACTI, University of Vigo) combined with a catalytic high-temperature combustion analyser (multi-N/C 3100 Autoanalyzer, Analytik Jena).

Dissolved iron content was determined using a Varian Liberty RL sequential inductively coupled plasma atomic emission spectroscopy (ICP-AES) setup. Prior to analysis, samples underwent a 50:50 v/v dilution with HNO_3 to ensure full solubility of iron.

3. Results and discussion

3.1. Physicochemical characterization of manufactured composites electrodes

3.1.1. FT-IR analysis

Fig. S1 displays the FT-IR spectra of the 9 electrodes synthesized via the three different methods. As depicted in Fig. S1.A,B and C, the peaks observed at 634–642, 627–640, and 654–669 cm^{-1} are attributed to the NZVI deformation mode associated with the catalysts used, namely P-NZVI, HB-NZVI, and AC-NZVI electrodes, respectively [17]. Furthermore, the bands observed at 1547 cm^{-1} in AC-NZVI/CF, 1487 cm^{-1} in AC-NZVI/Ti and 1617 cm^{-1} in AC-NZVI/HP are attributed to the presence of the C = C double bond in the AC composition, which is associated with aromatic ring vibrations or surface oxides. Moreover, the carboxyl bond in AC-NZVI is indicated by the bands at 1216, 1245 and 1218 cm^{-1} in AC-NZVI/CF, AC-NZVI/Ti and AC-NZVI/HP electrodes, respectively [31]. Additionally, the peaks at 485, 447 and 406 cm^{-1} are assigned to the Si − O − Si bending vibration while the peaks at 985 ,1166 and 980 cm^{-1} are assigned to the Si − O stretching vibration of bentonite clay tetrahedral sheets in HB-NZVI/CF, HB-NZVI/Ti and HB-NZVI/HP electrodes, respectively [32]. The spectra acquired for AC-NZVI/CF, HB-NZVI/CF, and P-NZVI/CF electrodes display a significant peak at wavelengths 3367, 3355, and 3352 cm^{-1}, respectively (Fig. S1A). For AC-NZVI/Ti, HB-NZVI/Ti, and P-NZVI/Ti electrodes notable peaks are observed at wavelengths 3342, 3345, and 3356 cm^{-1} (Fig. S1B). Similarly, the spectra obtained for AC-NZVI/HP, HB-NZVI/HP, and P-NZVI/HP electrodes exhibit prominent peaks at wavelengths 3370, 3334, and 3349 cm^{-1}(Fig.S1C). These peaks correspond to the O-H tensile vibration of the H_2O molecule [33]. This indicates the hydrophilic nature of the electrodes, facilitating their catalytic activity in aqueous solutions [34]. In Fig. S1.A, the arrangement of three electrodes by supporting the catalyst on the CF surface are presented. The PTFE binder exhibits clear characteristic bands at 1151 and 1213 cm^{-1} in the AC-NZVI/CF electrode, 1169 and 1208 cm^{-1} for the HB-NZVI/CF electrode, and at 1159 and 1212 cm^{-1} for the P-NZVI/CF electrode [35]. The CF present in all three electrodes displays stretching vibrations of C–H in methyl and methylene groups within the range of 2800–2980 cm^{-1}, and stretching vibrations of C–C as well as C = C centred at approximately 1050–1100 cm^{-1} and 1580–1699 cm^{-1}, respectively [36]. In Fig. S1.B, the arrangement of three electrodes synthetized by method B is illustrated, where the catalyst is supported on the Ti foil. Notably, the PVDF binder displays distinct characteristic bands at 1433 and 1666 cm^{-1} in the AC-NZVI/Ti electrode, 1407 and 1668 cm^{-1} for the HB-NZVI/Ti electrode, and at 1404 and 1608 cm^{-1} for the P-NZVI/Ti electrode [37]. Additionally, the Ti foil exhibits clear characteristic bands at 1033 cm^{-1}, 1180 cm^{-1}, and at 1184 cm^{-1} for the AC-NZVI/Ti, HB-NZVI/Ti and P-NZVI/Ti electrodes, respectively [38]. The FTIR peaks of the electrodes synthesized using the hand-pressing technique are illustrated in Fig. S1C. Within these spectra, the PTFE binder showcases distinct characteristic bands at HB-NZVI/HP 1191 and 1209 cm^{-1} in the AC-NZVI/HP electrode, 1189 and 1207 cm^{-1} for the electrode, and at 1194 and 1208 cm^{-1} for the P-NZVI/HP electrode [39].

3.1.2. XRD analysis

In all XRD patterns, the peaks at 2θ values of 44.9–45.2°, 46.2–47.8°, and 45.3–46.9° in the Fig. 1. A, B and C, respectively, correspond to the diffraction angle of NZVI at the (110) crystal plane, suggesting the presence of NZVI [40]. The broad peak below 26.5-27° in HB-NZVI/CF, HB-NZVI/TI and HB-NZVI/HP electrodes corresponds to the (210) planes of bentonite clay [41]. The peak corresponding to the (002) plane shows intense peaks at 2θ of 20–30°, indicating the presence of AC in AC-NZVI/CF, AC-NZVI/Ti and AC-NZVI/HP electrodes [42]. In the AC-NZVI/CF, HB-NZVI/CF and P-NZVI/CF electrodes, strong diffraction peaks were observed at 2θ values of 27°, 26.8°, and 28°, respectively (Fig. 1A), corresponding to the diffraction angle of the graphite structure at the (002) crystal plane. This indicates the presence of PTFE polymer as the main CF electrode surface [43]. The high peak intensities suggests excellent crystallinity of the prepared electrodes [44]. Additionally, diffraction peaks at 34°, 32.9°, and 35° 2θ in the AC-NZVI/CF, HB-NZVI/CF and P-NZVI/CF electrodes, respectively, correspond to secondary phases in the modified CF cathode at the (001) crystal plane, including iron hydroxides [45]. In the AC-NZVI/Ti, HB-NZVI/Ti and P-NZVI/Ti electrodes, strong diffraction peaks were observed at 2θ values of 20.17°, 21.08°, and 20.3°, respectively (Fig. 1B). These peaks correspond to the diffraction angle of the PVDF polymer as the main material on Ti foil, associated with the (003) plane [46]. Moreover, in the AC-NZVI/HP, HB-NZVI/HP and P-NZVI/HP electrodes, strong diffraction peaks were observed at 2θ values of 21.7°, 20.8°, and 21.2°, respectively (Fig. 1C), indicating the PTFE polymer as the main electrode surface, corresponding to the (002) plane [47].

3.1.3. XPS analysis

To gain a deeper understanding of the chemical composition and electronic structure of the nine composite electrodes, XPS analysis was conducted, with results presented in Fig. 2. The XPS survey spectra for the AC-NZVI/CF, HB-NZVI/CF and P-NZVI/CF electrodes (Fig. 2A) revealed pronounced peaks corresponding to carbon (C), oxygen (O), fluorine (F), and iron (Fe) at 294.6, 532.2, 689.5, and 728.4–825.3 eV, respectively [48]. This indicates the integration of these elements in the composite, particularly highlighting the presence of Fe on the electrode surface, which is crucial for the catalytic activity. For the AC-NZVI/Ti, HB-NZVI/Ti and P-NZVI/Ti electrodes (Fig. 2B), the spectra exhibited peaks for carbon (C), oxygen (O), fluorine (F), titanium (Ti) and iron (Fe), at 291.6, 528.2, 692.5, 408.45 and 736.4–818.3 eV, showing a clear presence of Ti in the composite structure, possibly contributing to the enhanced electrochemical properties [49]. In the AC-NZVI/HP, HB-

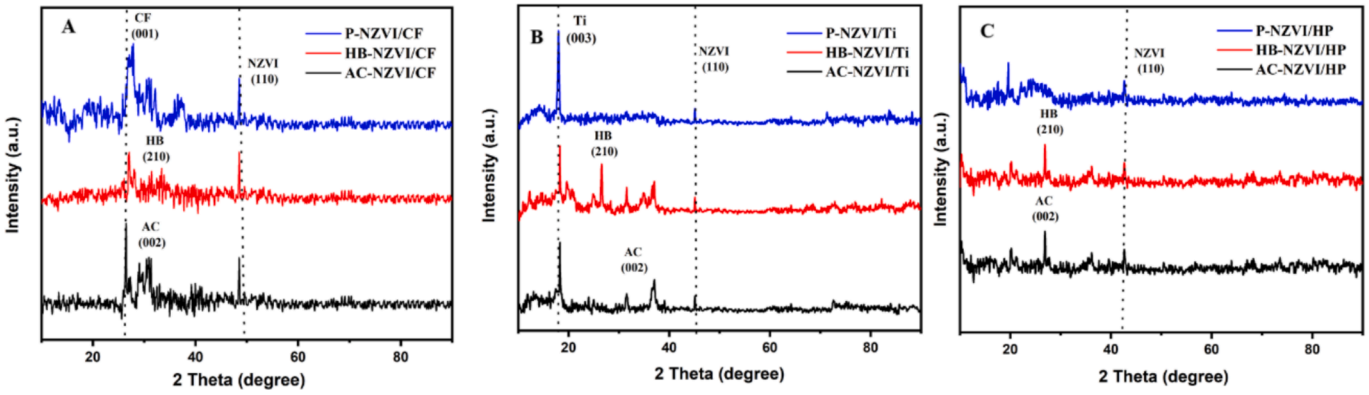

Fig. 1. XRD pattern of the synthesized electrodes using A, B and C methods.

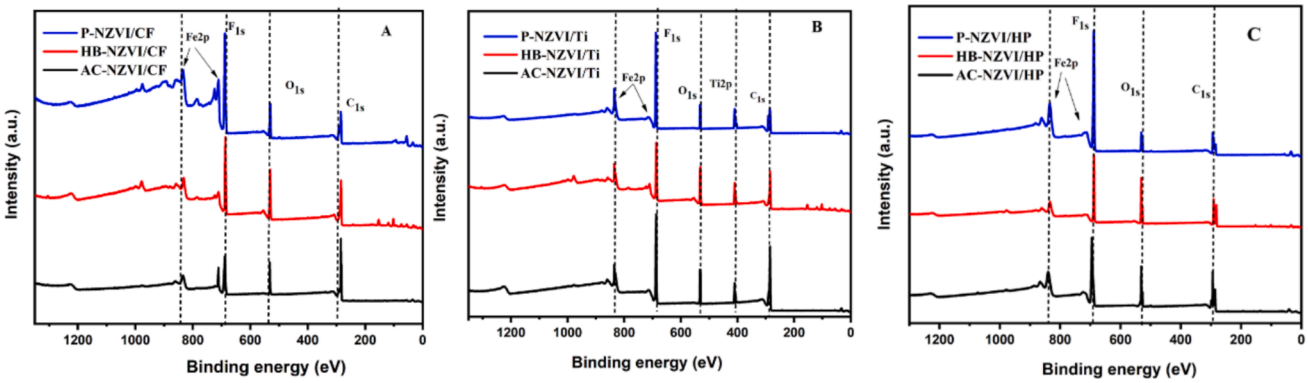

Fig. 2. XPS survey of 9 manufactured electrodes using A, B and C approaches.

NZVI/HP and P-NZVI/HP electrodes (Fig. 2C), the spectra show strong signals for carbon (C), oxygen (O), and fluorine (F) at 293.5, 526.5, and 688.5 eV, with a minor yet significant peak for iron (Fe) at 725–825.3 eV, indicating a lesser but significant presence of Fe [50]. The pronounced fluorine peaks are attributed to the polymer binders, PVDF and PTFE, which are integral to the composite's structure and contribute to its mechanical properties and chemical resistance [51]. This elemental distribution highlights the successful incorporation of the catalyst into the synthetized electrodes.

3.1.4. SEM-EDS analysis

The SEM evaluation of these electrodes, presented in Fig. 3, along with the EDS images in Figs. S2, S3, and S4, revealed a predominant presence of carbon, fluorine, iron, and oxygen in the AC-NZVI/CF, AC-NZVI/Ti, and AC-NZVI/HP electrodes, respectively. This indicates that these elements are the main components of all AC-NZVI materials. Then, HB-NZVI/CF (Fig.S2), HB-NZVI/Ti (Fig.S3) and HB-NZVI/HP (Fig.S4) electrodes show the presence of carbon, iron, silicon, fluorine, aluminium, and oxygen, highlighting the elements typical present on bentonites[14]. Similarly, the P-NZVI/CF (Fig.S2), P-NZVI/Ti (Fig.S3) and P-NZVI/HP (Fig.S4) substrates have a homogeneous distribution of iron, carbon, fluorine, and oxygen. Additionally, fluorine is detected, due to the PTFE and PVDF polymer binders used in the electrodes. The mapping analysis also successfully identified the Ti foil (Fig.S3) and CF (Fig.S2). All electrode samples exhibited a relatively smooth surface with a homogeneous distribution of carbon, oxygen, and iron, confirming the proper fixation of the catalyst in the composite. SEM analysis of the samples revealed spherical particles with hole-like structures in the electrodes fabricated by methods A Fig. 3(a,b,c) and B Fig. 3(d,e,f) [2,17,52] and chain-like structures in the samples prepared by method C Fig. 3(g,h,i) [47]. The elemental mapping images in Fig. S1, along with the SEM images in Fig. 3(a, b, c), illustrate the uniform distribution of AC-NZVI/CF (a, d), HB-NZVI/CF (b, e), and P-NZVI/CF (c, f) across the CF surface, in agreement with earlier reported studies[53].

3.2. Electrochemical characterization of composites electrodes manufactured

3.2.1. CV analysis

Fig. 4 displays the CV analysis of the nine manufactured electrodes. All samples demonstrated distinct oxidation peaks and indicated an irreversible process [54]; however, a notable potential shift of the oxidation peaks is observed for AC-NZVI/CF, HB-NZVI/CF and P-NZVI/CF, with the peak potential at 1.7 V. Among them, the AC-NZVI/CF composite electrode exhibited higher electro-catalytic activity compared to the other electrodes. This enhanced activity is attributed to the distribution of iron loaded onto the surface of the AC catalyst on the surface of the CF. This result suggests that AC-NZVI/CF could have a good conductivity [55].

3.2.2. EIS analysis

EIS examines the relationship between a potential energy difference and the flow of electrons induced by an alternating current signal applied in an aqueous medium. EIS analysis was used for investigating the electrochemical properties of materials in aqueous solutions due to its ability to simulate system behaviour using an idealized circuit model [56]. EIS is commonly employed to examine the total impedance within an electrochemical cell. Fig. S5 reveals the Nyquist plots of 9 electrodes in a frequency range from 10^{-1} to 10^{6} Hz. The Nyquist plots illustrate the imaginary portion (−Z") relative to the real part (Z') of the resistance (impedance), typically displaying a semi-circular pattern of all EIS plots. The X-intercept of the Nyquist plot, indicating the equivalent series

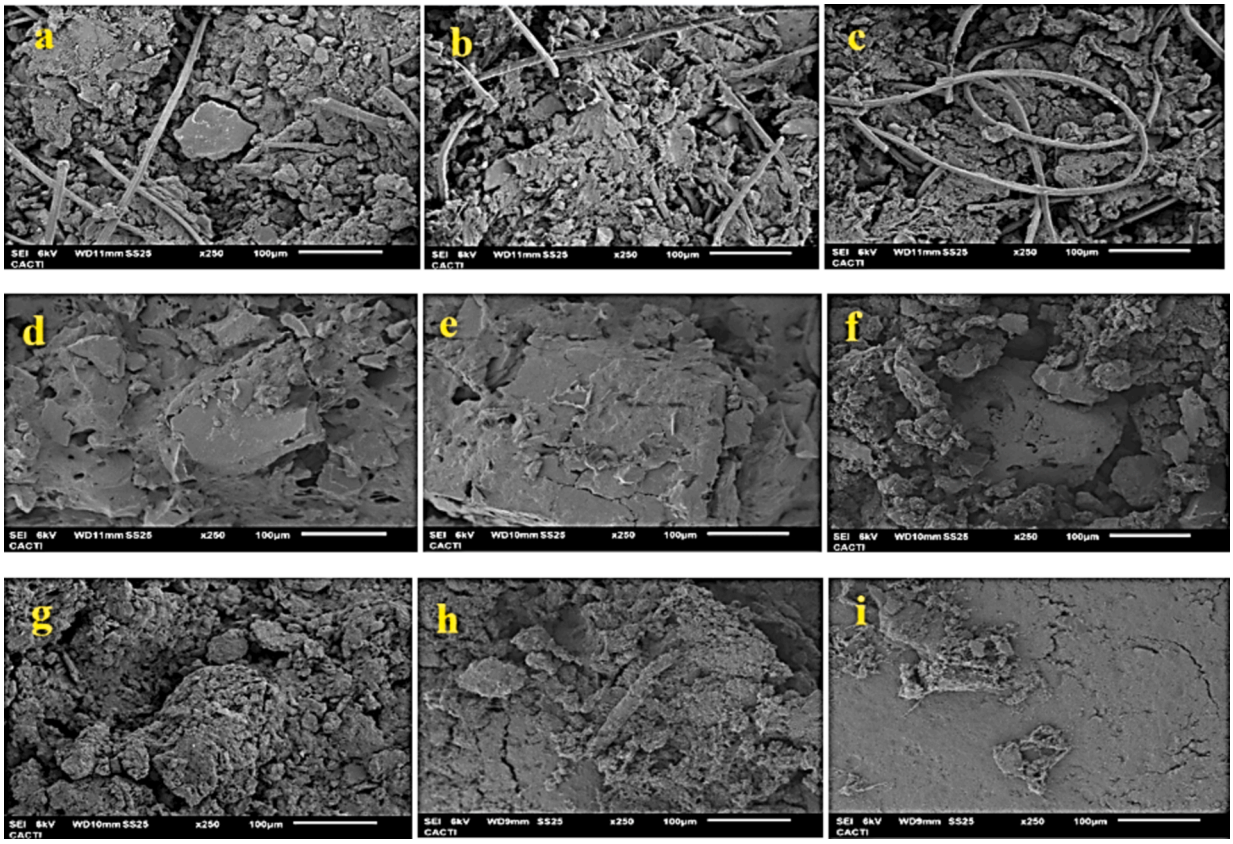

Fig. 3. SEM images of 9 manufactured electrodes using A, B and C approaches.

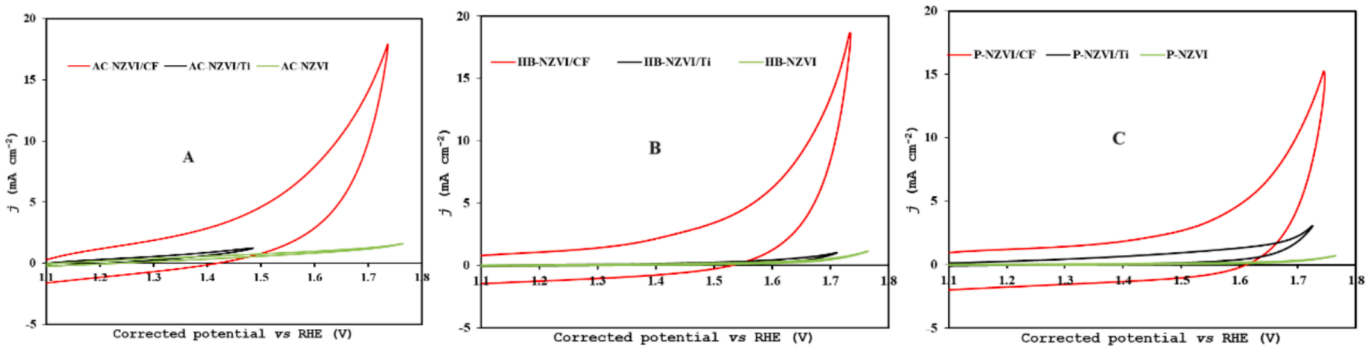

Fig. 4. CV (a), (b) and (c) for the blend electrode manufactured using A, B and C approaches, respectively on Ni-Foam in a three-electrode electrochemical cell with Na_2SO_4 0.5 M.

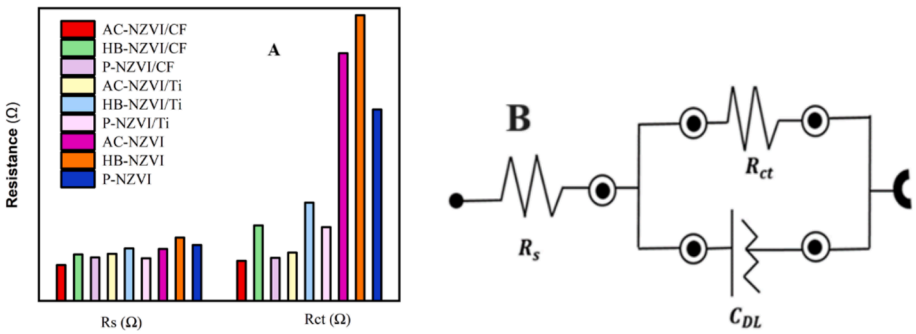

Fig. 5. (a) Histogram of simulated values for R_s and R_{ct} (b) equivalent circuit model of manufactured electrodes.

resistance (R_S) [57], defines an important parameter in EIS. Upon fitting EIS spectra with an equivalent electric circuit (see Fig. 5b), it becomes evident that AC-NZVI/CF electrode exhibits a lower R_S value of 2.28 Ω, attributed to enhanced conductivity compared to other electrodes (as depicted in Fig. 5a). Notably, the Nyquist plot illustrates a small semicircle at high frequency regions, the diameter of which correlates with the charge-transfer resistance (R_{ct}) of redox reactions [58]. Upon comparing the semicircle diameters of three electrodes, each utilizing the same catalyst under three different methods, it is inferred that the charge transfer resistance (R_{ct}) of AC-NZVI/CF electrode, synthesized using a specific technique supported onto the surface of a CF, is smaller than that of AC-NZVI/Ti electrode, synthesized via a method involving painting onto the surface of Ti, and the R_{ct} of AC-NZVI/HP electrode, prepared by hand pressing technique. These results indicate that AC-NZVI/CF is the most effective alternative, as it consistently demonstrates superior performance compared to other configurations. Across all nine scenarios, the electrodes of the AC-NZVI/CF electrode exhibit superior performance, suggesting favourable characteristics in conductivity and charge transfer.

EIS analysis corroborates the findings of CV analysis. The EIS measurements reveal that samples with a PTFE binder exhibit higher conductivity compared to those with a PVDF binder. The material AC-NZVI utilized in the experimental setup plays a crucial role in the synthesis of electrodes. This significance stems from the specific surface area of AC; according to literature, this area is pivotal in determining the electrochemical properties of AC in cathode synthesis [59]. The heightened surface area of AC is particularly crucial for high-performance conductivity applications. Additionally, the distribution of pore sizes can also impact conductivity performance [60]. The formation of a composite by optimally combining AC-NZVI with a PTFE polymer binder on the CF surface offers a cost-effective approach to generating cathode materials with excellent electrochemical performance in EFL applications.

3.3. EFL tests of manufactured electrodes on ATP degradation

Before the electrolysis was started, no adsorption of ATP on all tested electrodes was occurred within 30 min. Therefore, the subsequent ATP removal when electrolysis was started, was caused by electrochemical oxidation.

In order to compare the efficiency of the synthesized electrodes by method A, B and C, towards ATP degradation, a series of electrolysis tests were carried out while maintaining constant the initial ATP concentration of 40 mg/L at pH 3, $Na_2SO_4 = 0.05$ M, J = 25 mA/cm^2 for 60 min.

Fig. 6 A, B, and C show the ATP degradation with the nine synthesized electrodes. The AC-NZVI/CF cathode led to an ATP removal efficiency of 51 %, surpassing the HB-NZVI/CF and P-NZVI/CF cathodes, which gave removal efficiencies of 42 % and 35 %, respectively (Fig. 6A). This finding is in good agreement with the better electrochemical properties of the AC-NZVI/CF electrode which, as previously demonstrated, presents the lowest Rs value and the highest electrocatalytic activity compared to the other synthesized electrodes.

Similarly, the AC-NZVI/HP electrode demonstrated a removal efficiency of 40 % compared to 35 % and 27 % achieved with the HB-NZVI/HP and P-NZVI/HP electrodes, respectively (Fig. 6C). Fig. 6 A, B, and C show the ATP degradation with the nine synthesized electrodes. The AC-NZVI/CF cathode led to an ATP removal efficiency of 51 %, surpassing the HB-NZVI/CF and P-NZVI/CF cathodes, which gave removal efficiencies of 42 % and 35 %, respectively. This is consistent with the electroactivity demonstrated previously (Sections 3.2.). Similarly, the AC-NZVI/HP electrode demonstrated a removal efficiency of 40 % compared to 35 % and 27 % obtained with the HB-NZVI/HP and P-NZVI/HP electrodes, respectively (Fig. 6C). In the same way, the AC-NZVI/Ti electrode exhibited a 31 % of removal degradation rate, higher than that observed with the HB-NZVI/Ti and P-NZVI/Ti electrodes, reaching 25 % and 22 %, respectively (Fig. 6B).

The observed results provide meaningful information. On one hand, there is a significant effect of the selected binder on the ATP degradation performance. This can be attributed to the beneficial effect of PTFE/CB modification compared to PVDF/CB in enhancing *in-situ* H_2O_2 generation [61]. This is likely to happen due to the hydrophobic nature of PTFE, which facilitates the mass transfer of oxygen molecules, consequently boosting *in-situ* H_2O_2 production [62]. Numerous studies have shown that modification with PTFE/CB enhances electron transfer, leading to the reduction of oxygen at the cathode and subsequent *in-situ* H_2O_2 production [63]. On the other hand, the catalytic material added had a significant effect on all the essayed electrodes (Fig. 6). Specifically, AC-NZVI supported on CF not only activates molecular oxygen to generate *in-situ* H_2O_2 through a two-electron transfer reduction pathway [64] but also serves as a source for controlled release of ferrous ions, which catalyse the decomposition of *in-situ* produced H_2O_2 to generate $HO^{\bullet}$ [6]. Therefore, the electrode AC-NZVI/CF demonstrates the highest efficacy in electrochemical treatment, and consequently it was subjected to further investigations on ATP degradation.

3.4. ATP degradation using AC-NZVI/CF electrodes as cathode

3.4.1. Kinetic studies

Fig. S6 illustrates the linear kinetic plots for ZO (a), PFO (b), and PSO (c) models. The PFO model showed the best fit with the highest R^2 values (Table S3). In addition, the initial concentration (C_0) calculated with the PFO model closely matched the experimental value of 40 mg/L. The PFO model is therefore the most suitable to described ATP degradation in the EFL system using CF and AC-NZVI/CF electrodes. Other studies have also shown that the PFO model is well suited to describe ATP degradation [2,36].

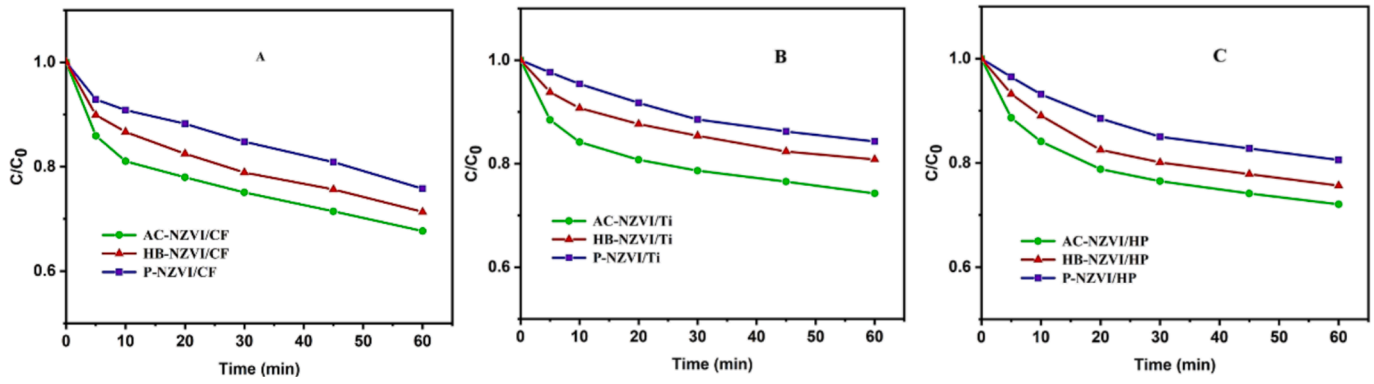

Fig. 6. Degradation profiles of ATP using various cathode manufacturing methods, ([ATP] = 40 mg/L, room temperature, pH 3, $Na_2SO_4 = 0.05$ M, J = 25 mA/cm^2, electrode manufactured/BDD).

3.4.2. H_2O_2production and ATP degradation utilizing CF and AC-NZVI/CF electrodes as cathode

The optimal synthetized electrode (AC-NZVI/CF) compared to support CF were utilized in the electro-catalytic process to compare their efficiency in generating H_2O_2. All experiments were conducted with a current density of 25 mA/cm^2, [ATP] = 40 mg/L at pH 3 for 150 min. Based on the data depicted in Fig. 7A, it is evident that the CF electrode exhibited higher H_2O_2 concentration reaching 0.211 mM compared to the AC-NZVI/CF electrode, attaining 0.159 mM of H_2O_2 concentration. This variance can be attributed to the catalysts present on the surface of the AC-NZVI/CF electrode, which promoted the decomposition of H_2O_2 generated on the electrode surface, leading to the generation of HO$^•$ radicals and then reducing the H_2O_2 concentration. Consequently, as illustrated by Fig. 7B, the AC-NZVI/CF electrode achieved a significantly higher ATP removal rate, reaching 65 %, while the CF electrode, using anodic oxidation, only achieved 47 %. Likewise, the rate constant of AC-NZVI/CF is higher than that of CF, with values of 0.5490 and 0.3230 min^{-1}, respectively, obtained using PFO models. The superiority of the heterogeneous AC-NZVI electro-catalyst, synthesized by incorporating it into CF as cathode electrode, has been established. The electrode preparation method involving the addition of CB, AC-NZVI, and PTFE to the CF significantly enhanced its capability to generate H_2O_2, surpassing that of unmodified CF by more than twice. Moreover, the presence of the AC-NZVI catalyst on the cathode facilitated the anticipated generation of HO$^•$ [65], favouring ATP degradation. Introducing NZVI enhances the electronic distribution within the catalyst, thereby accelerating electron transfer rates and consequently boosting the activation of H_2O_2 [66]. This observation led to the conclusion that the optimal production of H_2O_2 and degradation yields were achieved when using AC-NZVI/CF electrode as the cathode. In comparison to traditional EFL processes,

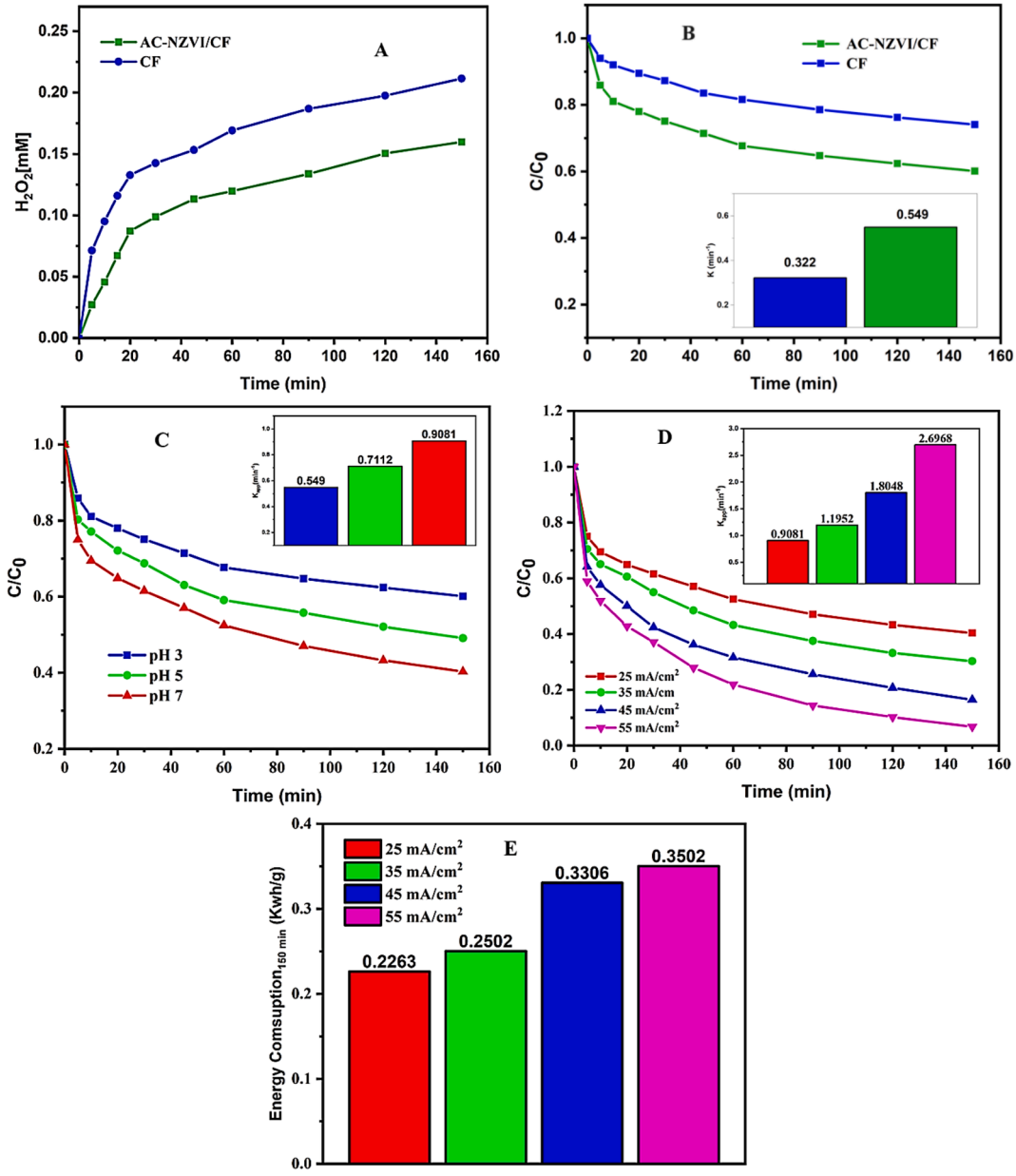

Fig. 7. (A) H_2O_2 evolution and (B) ATP removal efficiency utilizing different cathode ([ATP] = 40 mg/L, room temperature, pH 3, Na_2SO_4 = 0.05 M, J = 25 mA/cm^2), (C) Effect of pH on the removal of ATP ([ATP] = 40 mg/L, room temperature, J = 25 mA/cm^2, Na_2SO_4 = 0.05 M, AC-NZVI/FC-BDD), (D) Effect of current density on the removal of ATP and (E) Histogram of Energy consumption ([ATP] = 40 mg/L, room temperature, pH 7, Na_2SO_4 = 0.05 M, AC-NZVI/FC-BDD), (F) Removal and (G) TOC mineralization of water matrices on the ATP degradation ([ATP] = 40 mg/L, room temperature, J = 55 mA/cm^2, Na_2SO_4 = 0.05 M, pH 7, AC-NZVI/FC-BDD).

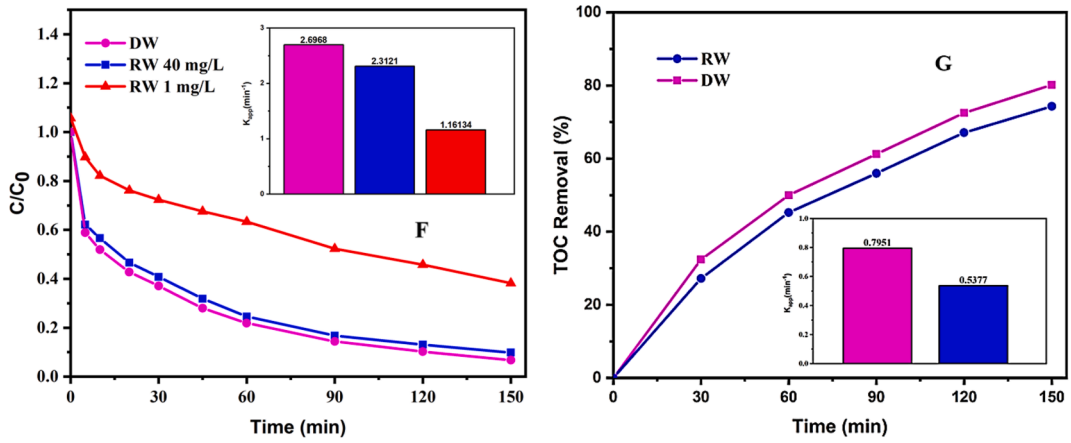

Fig. 7. (*continued*).

AC-NZVI catalyst supported on CF electrode demonstrates superior H_2O_2 production efficiency, with a yield of 0.159 mM in 150 min, which is higher than that reported for NZVI-based electrodes in similar systems [27,67]. Additionally, the degradation efficiency of ATP in our system reached 65 % of degradation in 150 min, compared to 60 min in homogeneous EF systems using Fe^{2+} catalysts [68].

3.4.3. Effect of pH

As an important parameter of the EFL process, the effect of initial pH values on the ATP degradation efficiency was studied (Fig. 7C). The composite electrode demonstrated ATP degradation efficiencies of 65 % and 72 % at pH values of 3 (0.5490 min^{-1}) and 5 (0.7112 min^{-1}), respectively. Under neutral pH conditions, the average ATP removal efficiency was consistently high at 81 %, with the highest apparent reaction rate of 0.9081 min^{-1}. Compared to the operational acid pH of conventional EFL processes, using AC-NZVI/CF as an electrode demonstrated robust ATP degradation capabilities under both neutral and acidic conditions, significantly expanding the applicable pH range of the system. The superior performance of the system stems from several key factors. Firstly, the presence of metal ions in solid form serves to prevent catalytic deactivation triggered by pH increases, ensuring sustained activity over time. Secondly, the reduction of Fe^{3+} to Fe^{2+} is notably boosted through cathodic reduction processes, enhancing the overall efficiency of the system. Thirdly, the Fe^{3+}/Fe^0 redox reaction plays a pivotal role in expediting electron transfer rates, thereby facilitating rapid catalytic reactions [69,70]. Considering these results, subsequent experiments were settled at initial pH of 7.

3.4.4. Effect of current density

The performance of the AC-NZVI/CF electrode was evaluated across various current densities ranging from 25 to 55 mA/cm^2, while maintaining constant operational conditions including an initial ATP concentration of 40 mg/L, room temperature, pH 7, and Na_2SO_4 concentration of 0.05 M. The ATP removal profiles over a 150 min duration are illustrated in Fig. 7D. Higher current densities resulted in higher removal rates of ATP and increased energy consumption. It is evident from the results that the rate of ATP removal escalated with increasing current density, achieving complete elimination within 150 min at a current density of 55 mA/cm^2 equivalent to 220 mA current intensity. This phenomenon can be attributed to the improvement of the electron transport process, which accelerates the reaction rate of EFL. Moreover, at elevated current densities, cathodic regeneration and electro-generation of Fe^{2+} from Fe^{3+} ions are facilitated, predominantly increasing the production of H_2O_2 /$HO^{\bullet}$ oxidative species [13]. Therefore, a current density of 55 mA/cm^2 with an energy requirement of 0.35 kWh/g (Fig. 7E) with PFO constant rate being 2.6968 min^{-1} was identified as the optimal applied condition for this EFL system. Further current increase was not contemplated, in order to avoid additional energy consumption. Conversely, other authors reported over ten times higher energy consumption using modified CF cathodes with surface areas of 14 cm × 5 cm, 17.5 cm × 6 cm, and 70 cm^2, and current intensities of 300 mA, 200 mA, and 300 mA, respectively [71–73].

3.4.5. Treatment of real wastewater

While fundamental research in synthetic water is crucial for understanding the mechanisms of electrochemical water remediation through EFL, it is equally very important to conduct catalytic assays in real water (RW) matrices. In real-world scenarios, the water matrix is a parameter that cannot be controlled and may significantly influence the selected treatment, owing to the presence of other species that can scavenge reactive radical species responsible for degrading the target pollutant [74]. Hence, the efficacy of a cathode based on AC-NZVI/CF for EFL treatment of ATP in a RW matrix was investigated. Water collected from the effluent of a municipal wastewater treatment plant in Guillarei (Spain) was spiked with 40 mg/L of ATP. Data presented in Fig. 7F illustrates the degradation of ATP over time, comparing data obtained in distilled water (DW) with that in RW effluent at the same initial concentration. Indeed, it was observed that 95.7 % and 94.48 % degradation of ATP was achieved after 150 min in both DW and RW effluent, respectively. The apparent rate constants (K_{app}) for the degradation were 2.6968 $min^{-1}$for DW and 2.3121 min^{-1} for RW, indicating the kinetic efficiency of the process.

Likewise, under the same electrochemical conditions, the removal efficiency of ATP at 1 mg/L in surface water reached 64 % (K_{app} = 1.1613) after 150 min (Fig. 7(F)). This highlights the need to optimize operational conditions at different pollutant concentrations, particularly in complex water matrices, to enhance reactive oxygen species generation.

The reduced performance at 1 mg/L may result from scavenging effects caused by excess oxidants reacting with each other instead of the pollutant, as reported in similar studies [27,75]. Nevertheless, these results remain competitive compared to previous works that achieved comparable removal rates under similar conditions or required higher intensities, which may increase the energy consumption [76]. This reinforces the potential of our optimized electrode for efficient pollutant degradation.

Similarly, significant mineralization rates were achieved in both water matrices, as shown in Fig. 7G. In 150 min, 75 % and 80 % mineralization of ATP were achieved in RW effluent and DW, respectively. This TOC reduction surpasses the 60–65 % reductions reported by others using modified CF as a cathode and BDD as an anode under similar conditions [77,78]. These results highlight the potential of AC-NZVI/CF as an effective cathode for treating pollutants through heterogeneous EFL treatments in both DW and RW matrices. While real

wastewater typically contains much lower concentrations of pharmaceutical pollutants, 40 mg/L ATP concentration applied in this study as a stress test for the electrode's catalytic performance under challenging conditions. This higher concentration allows for clear, measurable results and demonstrates the electrode's efficiency, stability, and resilience.

The cost-effectiveness, eco-friendliness, and high availability of carbon-supported NZVI emphasize the importance of further research into these materials as cathodes in EFL. They offer substantial economic advantages over conventional CF without compromising catalytic performance.

3.5. Recycle and stability of AC-NZVI/CF electrode

Fig. 8 illustrates the stability and reusability of the AC-NZVI/CF electrode as a cathode over five cycles for ATP degradation in RW. The physical and chemical properties of the catalyst play a crucial role in maintaining the catalytic activity across cycles. Following each cycle, the cathode underwent a gentle washing procedure with ultrapure water and ethanol, followed by drying for 12 h at 80 °C before being reused. The complete degradation of a 40 mg/L ATP solution was consistently achieved within 150 min across the five cycles (Fig. 8A), revealing the excellent stability of the AC-NZVI/CF electrode. This high stability can be attributed to the robust structure of the AC-NZVI catalyst supported on the CF surface. The strong interaction between AC-NZVI particles and the CF substrate contributes to the minimal leaching of iron, with leached iron concentrations of 0.021 mg/L after the first cycle (C1) and 0.032 mg/L after the fifth cycle (C5). The low iron leaching, approximately 9 % for C1 and 13 % for C5, indicates strong immobilization of the AC-NZVI catalyst on the CF substrate. These values are lower than those observed in our previous study, where AC-NZVI was used as a heterogeneous catalyst in the EFL process [2]. This finding demonstrates that the bonding between the catalyst and support is crucial for reusability, ensuring the environmental safety and sustainability of the process [79]. Additionally, after the first cycle (C1), a 70 % removal efficiency of TOC was achieved within 150 min, and after five cycles (C5), approximately 61 % TOC degradation efficiency was maintained. This slight decrease in TOC removal efficiency can be correlated with the progressive surface oxidation observed in the electrode material, as revealed by FTIR, XPS, and SEM-EDS analysis.

Fig. 8B illustrates the FTIR spectroscopy results for the AC-NZVI/CF electrode after undergoing the C1 and C5 cycles of the EFL process. The analysis reveals that the O-H stretching peaks experienced a notable shift, moving from 3367 cm^{-1} to 3394 cm^{-1} in C1 and to 3398 cm^{-1} in C5. This shift indicates changes in the hydrogen bonding environment of the O-H groups. Besides the peak shifts, the FTIR spectra indicates that carboxylic acids and their salts form metal-carboxylate complexes on the electrode surface, weakening the O-H antisymmetric stretching bands due to metal binding [80]. These observed changes in the hydrogen bonding environment of O-H groups, as well as the formation of metal-carboxylate complexes, suggest significant chemical modifications on the electrode surface. These modifications are likely responsible for the slight reduction in catalytic performance, as they alter the surface chemistry of the electrode. The shifts in O-H peaks and the weakening of

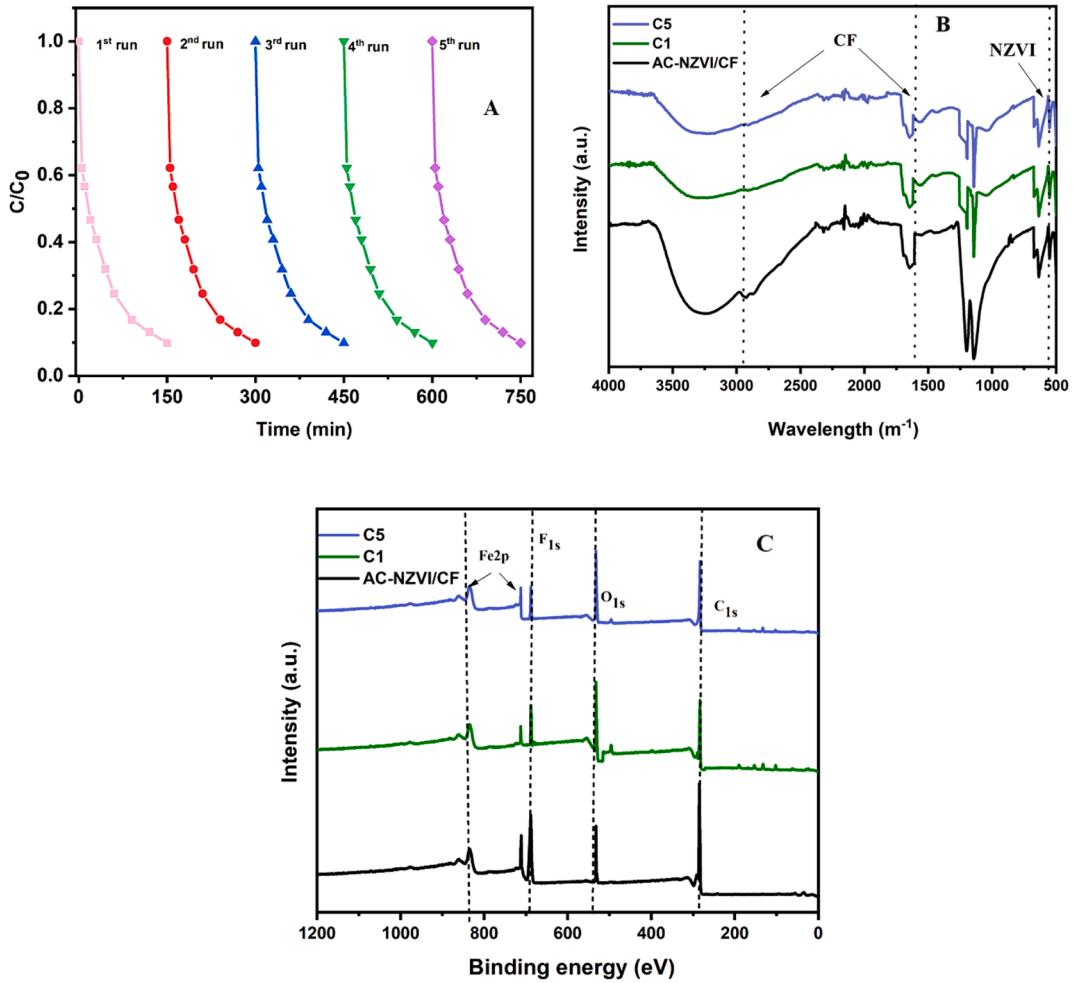

Fig. 8. (A) Consecutive runs of AC-NZVI/CF electrode as cathode for ATP removal from RW, (B) FTIR analysis of AC-NZVI/CF electrode after C1 and C5 EFL process, (C) XPS surveys of AC-NZVI/CF electrode before EFL process and after C1 and C5 EFL process.

O-H bands due to metal binding highlight how the surface chemistry changes progressively during the EFL process, influencing the reactivity and stability of the AC-NZVI/CF cathode. XPS analysis revealed significant alterations in the surface chemistry of the electrode following its operational cycles (Fig. 8.C). The O1s peak intensity exhibited a pronounced enhancement, indicating a substantial increase in oxygen-containing functional groups on the electrode surface caused during the oxidation process, which attacks the catalyst surface. Simultaneously, the C1s peak intensity showed a slight reduction, suggesting a decrease in carbon content. In addition, the F1s peak intensity experienced a notable decline, while the Fe 2p peak intensity remained relatively stable, indicating stabilization of the iron content. Quantitatively, the carbon content dropped from 47.12 % in the initial state to 41.41 % after C1, and further to 40.32 % after C5. Conversely, the content of H–O–H (water-related species) showed a significant increase, rising from 10.87 % initially to 20.83 % after C1, and to 22.42 % after C5, demonstrating a wettability increase due to the increase on functional groups on the surface [48]. The XPS C1s spectrum of the AC-NZVI/CF electrode (Fig. S7A) reveals five distinct peaks corresponding to C-H bonding (283.23 eV), Csp^2 and Csp^3 in the CF structure (284.86 eV), C–C bonding (284.7 eV), C–O bonding (286.35 eV), and C = O bonding (287.8 eV) [81,82]. Following EFL treatment, additional peaks attributed to –COOH and –O-C = O appear at the binding energy positions of 286.43 eV and 287.94 eV for C1 (Fig.S7B) and of 286.56 eV and at 288.7 eV for C5 (Fig.S7C) [83]. In the high-resolution XPS spectrum of the O 1 s region for the AC-NZVI/CF electrode, three distinct peaks are observed. The dominant peak at a binding energy of 534.7 eV is attributed to the C = O functional group. Additionally, peaks at 533.5 eV also correspond to C = O groups, while a shoulder peak at 530.28 eV is associated with COOH groups (Fig.S7D) [84]. However, following EFL treatment of the AC-NZVI/CF electrode, significant changes are observed in the O 1 s spectrum in Figs. Fig.S7E after C1 and in Fig.S7F after C5. The intensity of the C–O signal increases, while the peaks for C = O and COOH decrease markedly. This suggests that the C = O and COOH groups are being converted into hydroxyl (C–OH) groups on the surface of the AC-NZVI/CF electrode [22]. The generation of new C–OH bonds indicates a surface modification process induced by the EFL treatment, highlighting the dynamic nature of surface chemistry under electrochemical conditions [85]. The XPS analysis further corroborates these changes, showing a substantial increase in oxygen-containing functional groups, particularly C–OH bonds, which enhance the hydrophilicity of the electrode and contribute to improved electrochemical performance. However, this progressive oxidation could also explain the slight decline in TOC removal efficiency [48]. The observed modifications indicate a progressive oxidation process occurring on the surface of the electrode material. This oxidative environment could promote the adsorption or adhesion of ATP molecules, or intermediate products resulting from ATP degradation, onto the surface of the AC-NZVI/CF electrode [77]. The SEM-EDS images confirmed the presence of iron, carbon, and oxygen on the electrode surface after C1 (Fig.S8. a,c,e) and C5 (Fig.S8. b,d,f) cycles, with a notable reduction in fluorine content and an increase in oxygen compared to Fig. S1 (a, d, g). The oxidative changes observed in the electrode's surface chemistry correlate with its high stability, as they suggest that the AC-NZVI particles remain strongly bonded to the CF support despite the progressive oxidation of the surface [86]. These changes were corroborated by XPS analysis, which provided a detailed elemental composition of the electrode's surface. The emergence of cracks in the CF structure after five cycles indicates a slight decline in mechanical integrity due to physical stress from repeated use. Nevertheless, the electrode's ability to withstand oxidation and surface changes without losing catalytic activity underscores its durability for real-world applications. The strong bonding between AC-NZVI particles and the CF substrate in neutral pH conditions ensures both structural stability and effective pollutant degradation, making it a reliable choice for wastewater treatment [27]. While traditional electro-Fenton processes typically favour acidic conditions for efficient hydroxyl radical ($HO^{\bullet}$) generation [87], this study found that neutral pH conditions are more beneficial for pollutant degradation with the AC-NZVI/CF electrode. This advantage is likely attributed to the enhanced stability of the electrode in neutral environments, which reduces iron leaching and preserves the catalyst's activity over multiple cycles. Furthermore, neutral conditions facilitate the formation of other reactive oxygen species, such as superoxide anions [88], that contribute to pollutant breakdown, while also offering practical benefits like reduced corrosion and fewer pH adjustments for more sustainable treatment.

4. Conclusions

In conclusion, this study demonstrates the successful development of environmentally friendly cathodic electrodes for the EFL treatment of wastewater. Through the utilization of polymers such as PVDF and PTFE as binders, coupled with sustainable synthesis methods, it is possible to achieve efficient *in-situ* H_2O_2 generation and integration of heterogeneous catalysts, including AC-NZVI, HB-NZVI, and P-NZVI. Under optimal conditions, the AC-NZVI/CF electrode achieved 80 % mineralization of 40 mg/L ATP at pH 7 in 150 min, with an energy consumption of 0.3502 kWh/g. The kinetics of the ATP degradation followed a PFO, with a rate constant 2.6968 $min^{-1}$for DW and 2.312 min^{-1} for RW. The AC-NZVI/CF electrode demonstrated superior performance in ATP degradation than CF electrode, achieving 95 % degradation efficiency within 150 min. The stability and recyclability of the AC-NZVI/CF cathode were validated through comprehensive FTIR, SEM-EDS, and XPS analyses. The performance of EFL process was slightly affected in RW and remained consistent over five cycles, underscoring the durability and effectiveness of the AC-NZVI/CF electrode for real-world wastewater treatment applications. Looking ahead, future research efforts can concentrate on upscaling the synthesis and application of these environmentally friendly cathodic electrodes for larger-scale wastewater treatment. Conducting pilot-scale studies will offer valuable insights into the feasibility and efficiency of deploying these electrodes in real-world wastewater treatment plants.

CRediT authorship contribution statement

Dhiss Tesnim: Writing – original draft, Visualization, Software, Methodology, Investigation, Formal analysis, Data curation, Conceptualization. **Aida M. Díez:** Writing – review & editing, Visualization, Validation, Supervision, Resources, Project administration, Investigation, Funding acquisition. **Hédi Ben Amor:** Writing – review & editing, Supervision, Funding acquisition. **M. Angeles Sanromán:** Writing – review & editing, Resources, Project administration, Funding acquisition. **Marta Pazos:** Writing – review & editing, Resources, Project administration, Funding acquisition.

Funding

This research has been funded by R&D Project PID2020-113667 GB-I00 funded by MICIU / AEI /https://doi.org/10.13039/501100011033, PCI2022-132941 funded by MCIN/AEI/https://doi.org/10.13039/501100011033, Xunta de Galicia and European Regional Development Fund (ED431C 2021-43) and AXA Research Fund (project H2-ZeroWaste). The researcher Aida M. Díez is grateful to Xunta de Galicia for the financial support obtained (ED481D-2023/015). Funding for open access charge: Universidade de Vigo/CISUG.

Declaration of competing interest

The authors declare that they have no known competing financial interests or personal relationships that could have appeared to influence the work reported in this paper.

Appendix A. Supplementary data

Supplementary data to this article can be found online at https://doi.org/10.1016/j.cej.2024.158099.

Data availability

Data will be made available on request.

References

[1] P.V. Nidheesh, H. Olvera-Vargas, N. Oturan, M.A. Oturan, in: Heterogeneous Electro-Fenton Process: Principles and Applications, Electro-Fenton Process, Springer Singapore, Singapore, 2017, pp. 85–110, https://doi.org/10.1007/698_2017_72.

[2] T. Dhiss, A.M. Díez, B.A. Hédi, M.A. Sanroman, M. Pazos, Sustainable removal of antipyrine from wastewater via an Eco-Friendly heterogeneous Electro-Fenton-like process employing Zero-Valent iron nanoparticles loaded activated carbon, Chem. Eng. J. 152494 (2024).

[3] Ö. Görmez, F. Görmez, B. Gözmen, Comparison of the heterogeneous GO-FePO4/electro-Fenton against the homogeneous Fe (II) ion and Fe (III)-oxalate complex/electro-Fenton for the degradation of metronidazole, J. Water Process Eng. 43 (2021) 102265.

[4] D. Liu, H. Zhang, Y. Wei, B. Liu, Y. Lin, G. Li, F. Zhang, Enhanced degradation of ibuprofen by heterogeneous electro-Fenton at circumneutral pH, Chemosphere 209 (2018) 998–1006, https://doi.org/10.1016/j.chemosphere.2018.06.164.

[5] J. An, N. Li, Q. Zhao, Y. Qiao, S. Wang, C. Liao, L. Zhou, T. Li, X. Wang, Y. Feng, Highly efficient electro-generation of H2O2 by adjusting liquid-gas-solid three phase interfaces of porous carbonaceous cathode during oxygen reduction reaction, Water Res. 164 (2019) 114933.

[6] M. Pimentel, N. Oturan, M. Dezotti, M.A. Oturan, Phenol degradation by advanced electrochemical oxidation process electro-Fenton using a carbon felt cathode, Appl. Catal. B Environ. 83 (2008) 140–149.

[7] W. Zhou, L. Rajic, L. Chen, K. Kou, Y. Ding, X. Meng, Y. Wang, B. Mulaw, J. Gao, Y. Qin, Activated carbon as effective cathode material in iron-free Electro-Fenton process: Integrated H2O2 electrogeneration, activation, and pollutants adsorption, Electrochimica Acta 296 (2019) 317–326.

[8] P. Cao, X. Quan, K. Zhao, S. Chen, H. Yu, J. Niu, Selective electrochemical H2O2 generation and activation on a bifunctional catalyst for heterogeneous electro-Fenton catalysis, J. Hazard. Mater. 382 (2020) 121102.

[9] A.C. Del Álamo, A. Puga, M.I. Pariente, E. Rosales, R. Molina, M. Pazos, F. Martínez, M.A. Sanroman, Activity and stability of bifunctional perovskite/carbon-based electrodes for the removal of antipyrine by electro-Fenton process, Chemosphere 334 (2023) 138858.

[10] E. López-Fernández, C.G. Sacedón, J. Gil-Rostra, F. Yubero, A.R. González-Elipe, A. de Lucas-Consuegra, Recent advances in alkaline exchange membrane water electrolysis and electrode manufacturing, Molecules 26 (2021) 6326.

[11] A. Huang, D. Zhi, Y. Zhou, A novel modified Fe–Mn binary oxide graphite felt (FMBO-GF) cathode in a neutral electro-Fenton system for ciprofloxacin degradation, Environ. Pollut. 286 (2021) 117310, https://doi.org/10.1016/j.envpol.2021.117310.

[12] S. Zhang, Z. Kong, H. Wang, Q. Yan, D.V. Vayenas, G. Zhang, Enhanced nitrate removal by biochar supported nano zero-valent iron (nZVI) at biocathode in bioelectrochemical system (BES), Chem. Eng. J. 433 (2022) 133535, https://doi.org/10.1016/j.cej.2021.133535.

[13] X. Ma, Z. Xu, L. Zhang, S. Sun, C. Liu, J. Zhang, F. He, P. Dong, C. Zhao, H. Sun, Nano zero-valent iron-based fiber electrode for efficient electro-Fenton treatment of pharmaceutical wastewater: Mechanism of degradation and sterilization, Chem. Eng. J. 475 (2023) 146049.

[14] L. Li, Y. Sun, L. Feng, Graphene Felt Electrode Modified by Montmorillonite Supported Nano-Zero-Valent Iron, Carbon Black and Ptfe for Efficient Heterogeneous Electro-Fenton Degradation of Ciprofloxacion, accessed November 7, Carbon Black Ptfe Effic. Heterog. Electro-Fenton Degrad. Ciprofloxacion (n.d.) (2023), https://papers.ssrn.com/sol3/papers.cfm?abstract_id=4114036.

[15] S. Panić, M. Petronijević, J. Vukmirović, N. Grba, S. Savić, Green synthesis of nanoscale zero-valent iron aggregates for catalytic degradation of textile dyes, Catal. Lett. 153 (2023) 3605–3619.

[16] A. Leovac Maćerak, A. Kulić Mandić, V. Pešić, D. Tomašević Pilipović, M. Bečelić-Tomin, D. Kerkez, "Green" nZVI-biochar as fenton catalyst: perspective of closing-the-loop in wastewater treatment, Molecules 28 (2023) 1425.

[17] T. Dhiss, B.A. Hedi, J. Simal-Gandara, Sustainable and Green Synthesis of Iron Nanoparticles Supported on Natural Clays via Palm Waste Extract for Catalytic Oxidation of Crocein Orange G Mono Azoic Dye, ACS Omega 8 (2023) 34364–34376, https://doi.org/10.1021/acsomega.3c01333.

[18] C. Zhang, F. Li, R. Wen, H. Zhang, P. Elumalai, Q. Zheng, H. Chen, Y. Yang, M. Huang, G. Ying, Heterogeneous electro–Fenton using three–dimension NZVI–BC electrodes for degradation of neonicotinoid wastewater, Water Res. 182 (2020) 115975.

[19] W.H. Wang, X.D. Wang, Investigation of Ir-modified carbon felt as the positive electrode of an all-vanadium redox flow battery, Electrochimica Acta 52 (2007) 6755–6762.

[20] V. Poza-Nogueiras, A. Gomis-Berenguer, M. Pazos, A. Sanroman, C.O. Ania, Exploring the use of carbon materials as cathodes in electrochemical advanced oxidation processes for the degradation of antibiotics, J. Environ. Chem. Eng. 10 (2022) 107506.

[21] J. Jiang, G. Li, Z. Li, X. Zhang, F. Zhang, An Fe–Mn binary oxide (FMBO) modified electrode for effective electrochemical advanced oxidation at neutral pH, Electrochimica Acta 194 (2016) 104–109.

[22] L. Zhou, M. Zhou, Z. Hu, Z. Bi, K.G. Serrano, Chemically modified graphite felt as an efficient cathode in electro-Fenton for p-nitrophenol degradation, Electrochimica Acta 140 (2014) 376–383.

[23] C.L. Zhu, C. Tao, J.J. Bao, Y.P. Huang, G.W. Xu, Waterborne Polyurethane Used as Binders for Lithium-Ion Battery with Improved Electrochemical Properties, Adv. Mater. Res. 1090 (2015) 199–204, https://doi.org/10.4028/www.scientific.net/AMR.1090.199.

[24] T. Sun, S. Wang, M. Xu, N. Qiao, Q. Zhu, B. Xu, High-Performance Sulfurized Polyacrylonitrile Cathode by Using MXene as a Conductive and Catalytic Binder for Room-Temperature Na/S Batteries, ACS Appl. Mater. Interfaces 16 (2024) 10093–10103, https://doi.org/10.1021/acsami.3c17874.

[25] J.F. Pérez, C. Sáez, J. Llanos, P. Cañizares, C. López, M.A. Rodrigo, Improving the Efficiency of Carbon Cloth for the Electrogeneration of H2O2: Role of Polytetrafluoroethylene and Carbon Black Loading, Ind. Eng. Chem. Res. 56 (2017) 12588–12595, https://doi.org/10.1021/acs.iecr.7b02563.

[26] A. Qureashi, A.H. Pandith, A. Bashir, L.A. Malik, T. Manzoor, F.A. Sheikh, K. Fatima, Z. Haq, Electrochemical analysis of glyphosate using porous biochar surface corrosive nZVI nanoparticles, Nanoscale Adv. 5 (2023) 742–755.

[27] M. Liu, Y. Ye, L. Xu, T. Gao, A. Zhong, Z. Song, Recent Advances in Nanoscale Zero-Valent Iron (nZVI)-Based Advanced Oxidation Processes (AOPs): Applications, Mechanisms, and Future Prospects, Nanomaterials 13 (2023) 2830.

[28] T. Dhiss, B.A. Hédi, D. Ridha, A. Cid-Samamed, Green low-cost synthesis of zero-valent iron nanoparticles from Palm Petiole Extract for Cr(VI) removal from water, Environ. Sci. Pollut. Res. (2024), https://doi.org/10.1007/s11356-024-34092-1.

[29] M.M. Jiad, A.H. Abbar, Treatment of petroleum refinery wastewater by an innovative electro-Fenton system: Performance and specific energy consumption evaluation, Case Stud. Chem. Environ. Eng. 8 (2023) 100431.

[30] R.M. Sellers, Spectrophotometric determination of hydrogen peroxide using potassium titanium (IV) oxalate, Analyst 105 (1980) 950–954.

[31] N. Abderrahim, M. Mergbi, H.B. Amor, R. Djellabi, Optimization of microwave assisted synthesis of activated carbon from biomass waste for sustainable industrial crude wet-phosphoric acid purification, J. Clean. Prod. 394 (2023) 136326.

[32] E. Annan, E. Nyankson, B. Agyei-Tuffour, S.K. Armah, G. Nkrumah-Buandoh, J.A. M. Hodasi, M. Oteng-Peprah, Synthesis and characterization of modified kaolin-bentonite composites for enhanced fluoride removal from drinking water, Adv. Mater. Sci. Eng. 2021 (2021) 1–12.

[33] J. Shi, H. Deng, L. Lu, F. Chen, H. Xu, S. Wang, F. Xu, Performance of nickel–zinc battery with ZnO/activated carbon/3D network carbon felt as zinc negative electrode, J. Appl. Electrochem. 51 (2021) 1675–1687, https://doi.org/10.1007/s10800-021-01611-8.

[34] S. Tanaka, S. Takaya, T. Kumeda, N. Hoshi, K. Miyatake, M. Nakamura, Tailoring the hydrophilic and hydrophobic reaction fields of the electrode interface on single crystal Pt electrodes for hydrogen evolution/oxidation reactions, Int. J. Hydrog. Energy 46 (2021) 28078–28086.

[35] B. Zhao, S. Sun, Y. Luo, Y. Cheng, Fabrication of polytetrafluoroethylene coated micron aluminium with enhanced oxidation, Materials 13 (2020) 3384.

[36] L. Chen, S. Yuan, H. Wang, Y. Zhu, D. Fu, Z. Li, Spherical Polydopamine-Modified Carbon-Felt Cathode with an Active Indole Structure for Efficient Hydrogen Peroxide Electroproduction, Appl. Sci. 11 (2021) 5371.

[37] S. Jia, J. Long, J. Li, S. Yang, K. Huang, N. Yang, Y. Liang, J. Xiao, Biomineralized zircon-coated PVDF nanofiber separator for enhancing thermo- and electrochemical properties of lithium ion batteries, J. Mater. Sci. 55 (2020) 14907–14921, https://doi.org/10.1007/s10853-020-05051-1.

[38] S.I. Jariya, N. Manivannan, B.M. Ali, T.S. Narayanan, K. Ravichandran, Engineering the surface of titanium to improve its bioactivity and antibacterial activity through a multi-functional coating approach, New J. Chem. 47 (2023) 5843–5862.

[39] J. Bitenc, T. Pavčnik, U. Košir, K. Pirnat, Quinone based materials as renewable high energy density cathode materials for rechargeable magnesium batteries, Materials 13 (2020) 506.

[40] S.O. Ganiyu, T.X.H. Le, M. Bechelany, N. Oturan, S. Papirio, G. Esposito, E. van Hullebusch, M. Cretin, M.A. Oturan, Electrochemical mineralization of sulfamethoxazole over wide pH range using FeIIFeIII LDH modified carbon felt cathode: Degradation pathway, toxicity and reusability of the modified cathode, Chem. Eng. J. 350 (2018) 844–855.

[41] R.S. Hebbar, A.M. Isloor, B. Prabhu, A.M. Inamuddin, A.F.I. Asiri, Removal of metal ions and humic acids through polyetherimide membrane with grafted bentonite clay, Sci. Rep. 8 (2018) 4665.

[42] M. Mergbi, D. Aboagye, S. Contreras, H.B. Amor, F. Medina, R. Djellabi, Fast g-C3N4 sonocoated activated carbon for enhanced solar photocatalytic oxidation of organic pollutants through Adsorb & Shuttle process, Ultrason. Sonochem. 99 (2023) 106550.

[43] B. Vasconcelos, R. Serra, J. Oliveira, C. Fonseca, Characterization and Tribological Behavior of Electroless-Deposited Ni-P-PTFE Films on NBR Substrates for Dynamic Contact Applications, Coatings 12 (2022) 1410, https://doi.org/10.3390/coatings12101410.

[44] Z. Zhou, F. Chen, T. Kuang, L. Chang, J. Yang, P. Fan, Z. Zhao, M. Zhong, Lignin-derived hierarchical mesoporous carbon and NiO hybrid nanospheres with exceptional Li-ion battery and pseudocapacitive properties, Electrochimica Acta 274 (2018) 288–297, https://doi.org/10.1016/j.electacta.2018.04.111.

[45] W. Achour, F. Ynineb, T. Hadjersi, F. Moulai, M. Ifires, A. Khen, A. Manseri, M. Kechouane, Hydrothermal deposition of urchin-like NiCo2O4 on carbon felt as performed flexible electrodes for supercapacitors, J. Appl. Electrochem. 53 (2023) 1405–1419, https://doi.org/10.1007/s10800-023-01863-6.

[46] Y. Ren, Y. Wang, W. Zhang, X. Yan, B. Huang, Improved battery performance contributed by the optimized phase ratio of β and α of PVDF, RSC Adv. 9 (2019) 29760–29764.

[47] C. Huang, Z. Zhang, L. Sun, J. Wang, Enhancing wear and corrosion resistance of electroless Ni-P coatings in CO2-saturated NaCl solution through polytetrafluoroethylene incorporation, Corros. Sci. 226 (2024) 111620.

[48] O. Di Blasi, N. Briguglio, C. Busacca, M. Ferraro, V. Antonucci, A. Di Blasi, Electrochemical investigation of thermically treated graphene oxides as electrode materials for vanadium redox flow battery, Appl. Energy 147 (2015) 74–81.

[49] B. Singh, S. Gautam, G.C. Behera, R. Kumar, V. Aggarwal, J.S. Tawale, R. Ganesan, S.C. Roy, S.S. Kushvaha, MoS2 thin film decorated TiO2 nanotube arrays on flexible Ti foil for solar water splitting application, Nano Express 5 (2024) 015006.

[50] X. Jia, G. Li, B. Liu, Y. Luo, G. Yang, X. Yang, Multiscale reinforcement and interfacial strengthening on epoxy-based composites by silica nanoparticle-multiwalled carbon nanotube complex, Compos. Part Appl. Sci. Manuf. 48 (2013) 101–109.

[51] P. Kaspar, D. Sobola, K. Částková, R. Dallaev, E. Šťastná, P. Sedlák, A. Knápek, T. Trčka, V. Holcman, Case study of polyvinylidene fluoride doping by carbon nanotubes, Materials 14 (2021) 1428.

[52] S. Panić, M. Petronijević, J. Vukmirović, N. Grba, S. Savić, Green Synthesis of Nanoscale Zero-Valent Iron Aggregates for Catalytic Degradation of Textile Dyes, Catal. Lett. 1–15 (2023).

[53] X.-J. Han, P.-X. Sun, W.-J. Pan, L.-J. Chen, Z.-J. Chen, Q. Zhang, J. Wang, C. Yang, Porous multi-layer MoO2/β-MnO2 composite cathode for phosphorylated glucose fuel cell, J. Solid State Electrochem. 25 (2021) 1861–1869, https://doi.org/10.1007/s10008-021-04954-6.

[54] E.M. Espinoza, J.A. Clark, J. Soliman, J.B. Derr, M. Morales, V.I. Vullev, Practical Aspects of Cyclic Voltammetry: How to Estimate Reduction Potentials When Irreversibility Prevails, J. Electrochem. Soc. 166 (2019) H3175, https://doi.org/10.1149/2.0241905jes.

[55] M. Gong, Case Study on the Reproducibility of Characterizing the Electrocatalytic Activity of La1- xSrxMnO3 in ORR, Crystals 13 (2023) 74.

[56] S. Wang, J. Zhang, O. Gharbi, V. Vivier, M. Gao, M.E. Orazem, Electrochemical impedance spectroscopy, Nat. Rev. Methods Primer 1 (2021) 41.

[57] N.O. Laschuk, E.B. Easton, O.V. Zenkina, Reducing the resistance for the use of electrochemical impedance spectroscopy analysis in materials chemistry, RSC Adv. 11 (2021) 27925–27936.

[58] Y. Wang, Y. Lei, J. Li, L. Gu, H. Yuan, D. Xiao, Synthesis of 3D-Nanonet Hollow Structured Co $_3$ $_O$ 4 for High Capacity Supercapacitor, ACS Appl. Mater. Interfaces 6 (2014) 6739–6747, https://doi.org/10.1021/am500464n.

[59] M. Li, H. Xiao, T. Zhang, Q. Li, Y. Zhao, Activated Carbon Fiber Derived from Sisal with Large Specific Surface Area for High-Performance Supercapacitors, ACS Sustain. Chem. Eng. 7 (2019) 4716–4723, https://doi.org/10.1021/acssuschemeng.8b04607.

[60] Y. Lu, S. Zhang, J. Yin, C. Bai, J. Zhang, Y. Li, Y. Yang, Z. Ge, M. Zhang, L. Wei, Mesoporous activated carbon materials with ultrahigh mesopore volume and effective specific surface area for high performance supercapacitors, Carbon 124 (2017) 64–71.

[61] S. Priyono, T.D. Sari, A. Subhan, B. Prihandoko, Effect of polymer binders on the electrochemical Performance of Al-doped lithium titanate electrode, in: J. Phys. Conf. Ser., IOP Publishing, 2019: p. 012056. https://iopscience.iop.org/article/10.1088/1742-6596/1282/1/012056/meta (accessed March 1, 2024).

[62] M. Li, X. Qin, M. Gao, T. Li, Y. Lv, Enhanced in-situ electrosynthesis of hydrogen peroxide on a modified active carbon fiber prepared through response surface methodology, J. Electroanal. Chem. 912 (2022) 116241.

[63] Y. Jiao, L. Ma, Y. Tian, M. Zhou, A flow-through electro-Fenton process using modified activated carbon fiber cathode for orange II removal, Chemosphere 252 (2020) 126483.

[64] Y. Cheng, W. Zhou, L. Zhu, Enhanced reactivity and mechanisms of mesoporous carbon supported zero-valent iron composite for trichloroethylene removal in batch studies, Sci. Total Environ. 718 (2020) 137256.

[65] A. Asghar, A.A.A. Raman, W.M.A.W. Daud, Advanced oxidation processes for in-situ production of hydrogen peroxide/hydroxyl radical for textile wastewater treatment: a review, J. Clean. Prod. 87 (2015) 826–838.

[66] M. Xu, J. Wei, X. Cui, J. Li, G. Pan, Y. Li, Z. Jiang, X. Niu, N. Cui, J. Li, High-efficiency electro-Fenton process based on in-situ grown CoFeCe-LDH@ CFs free-standing cathodes: Correlation of cerium and oxygen vacancies with H2O2, Chem. Eng. J. 455 (2023) 140922.

[67] A. Gopinath, L. Pisharody, A. Popat, P.V. Nidheesh, Supported catalysts for heterogeneous electro-Fenton processes: Recent trends and future directions, Curr. Opin. Solid State Mater. Sci. 26 (2022) 100981.

[68] A. Fdez-Sanromán, M. Pazos, M.A. Sanromán, E. Rosales, Heterogeneous electro-Fenton system using Fe-MOF as catalyst and electrocatalyst for degradation of pharmaceuticals, Chemosphere 340 (2023) 139942.

[69] M. Al-Badani, P.L. Chong, H.S. Lim, A mini review of the effect of modified carbon paper, carbon felt, and carbon cloth electrodes on the performance of microbial fuel cell, Int. J. Green Energy 21 (2024) 170–186, https://doi.org/10.1080/15435075.2023.2194979.

[70] T.X.H. Le, M. Bechelany, M. Cretin, Carbon felt based-electrodes for energy and environmental applications: A review, Carbon 122 (2017) 564–591.

[71] A. Özcan, A.A. Özcan, Y. Demirci, Evaluation of mineralization kinetics and pathway of norfloxacin removal from water by electro-Fenton treatment, Chem. Eng. J. 304 (2016) 518–526.

[72] H. Lin, N. Oturan, J. Wu, H. Zhang, M.A. Oturan, Cold incineration of sucralose in aqueous solution by electro-Fenton process, Sep. Purif. Technol. 173 (2017) 218–225.

[73] A. Özcan, A.A. Özcan, Y. Demirci, E. Şener, Preparation of Fe2O3 modified kaolin and application in heterogeneous electro-catalytic oxidation of enoxacin, Appl. Catal. B Environ. 200 (2017) 361–371.

[74] M.Y. Alazaiza, A. Albahnasawi, M. Eyvaz, D.E. Nassani, S.S. Abu Amr, M.S. S. Abujazar, O. Al-Maskari, Electrochemical-based advanced oxidation for hospital wastewater treatment, Desalin, Water Treat 300 (2023) 44–56.

[75] E.M. Cuerda-Correa, M.F. Alexandre-Franco, C. Fernández-González, Advanced oxidation processes for the removal of antibiotics from water, An Overview, Water 12 (2019) 102.

[76] J. Lee, G. Antonini, A. Al-Omari, C. Muller, J. Mathew, K. Bell, J.M. Pearce, D. Santoro, Electrochemical Methods for Nutrient Removal in Wastewater: A Review of Advanced Electrode Materials, Processes, and Applications. Sustainability 2024, 16, 9764, (2024). https://www.researchgate.net/profile/Giorgio-Antonini-2/publication/385717459_Electrochemical_Methods_for_Nutrient_Removal_in_Wastewater_A_Review_of_Advanced_Electrode_Materials_Processes_and_Applications_Electrochemical_Methods_for_Nutrient_Removal_in_Wastewater_A_Review_of_Ad/links/6732716b68de5e5a30739329/Electrochemical-Methods-for-Nutrient-Removal-in-Wastewater-A-Review-of-Advanced-Electrode-Materials-Processes-and-Applications-Electrochemical-Methods-for-Nutrient-Removal-in-Wastewater-A-Review-of.pdf (accessed November 23, 2024).

[77] J. Zhang, D. Wang, F. Zhao, J. Feng, H. Feng, J. Luo, W. Tang, Ferrate modified carbon felt as excellent heterogeneous electro-Fenton cathode for chloramphenicol degradation, Water Res. 227 (2022) 119324.

[78] T. Cui, Z. Xiao, Z. Wang, C. Liu, Z. Song, Y. Wang, Y. Zhang, R. Li, B. Xu, F. Qi, FeS2/carbon felt as an efficient electro-Fenton cathode for carbamazepine degradation and detoxification: In-depth discussion of reaction contribution and empirical kinetic model, Environ. Pollut. 282 (2021) 117023.

[79] W. Yang, M. Zhou, L. Liang, Highly efficient in-situ metal-free electrochemical advanced oxidation process using graphite felt modified with N-doped graphene, Chem. Eng. J. 338 (2018) 700–708.

[80] O. Karatas, N.A. Gengec, E. Gengec, A. Khataee, M. Kobya, High-performance carbon black electrode for oxygen reduction reaction and oxidation of atrazine by electro-Fenton process, Chemosphere 287 (2022) 132370.

[81] M. Schnucklake, L. Eifert, J. Schneider, R. Zeis, C. Roth, Porous N-and S-doped carbon–carbon composite electrodes by soft-templating for redox flow batteries, Beilstein J. Nanotechnol. 10 (2019) 1131–1139.

[82] S. Su, Y. Wang, J. Qin, C. Wang, Z. Yao, R. Lu, Q. Wang, Continuous method for grafting CNTs on the surface of carbon fibers based on cobalt catalyst assisted by thiourea, J. Mater. Sci. 54 (2019) 12498–12508, https://doi.org/10.1007/s10853-019-03827-8.

[83] G. Wu, L. Chen, L. Liu, Direct grafting of octamaleamic acid-polyhedral oligomeric silsesquioxanes onto the surface of carbon fibers and the effects on the interfacial properties and anti-hydrothermal aging behaviors of silicone resin composites, J. Mater. Sci. 52 (2017) 1057–1070, https://doi.org/10.1007/s10853-016-0401-y.

[84] C. Qiu, L. Jiang, Y. Gao, L. Sheng, Effects of oxygen-containing functional groups on carbon materials in supercapacitors: A review, Mater. Des. 111952 (2023).

[85] E.-M. Kirchner, T. Hirsch, Recent developments in carbon-based two-dimensional materials: synthesis and modification aspects for electrochemical sensors, Microchim. Acta 187 (2020) 441, https://doi.org/10.1007/s00604-020-04415-3.

[86] J. Li, D. Song, K. Du, Z. Wang, C. Zhao, Performance of graphite felt as a cathode and anode in the electro-Fenton process, RSC Adv. 9 (2019) 38345–38354.

[87] Y. Liu, Y. Zhao, J. Wang, Fenton/Fenton-like processes with in-situ production of hydrogen peroxide/hydroxyl radical for degradation of emerging contaminants: Advances and prospects, J. Hazard. Mater. 404 (2021) 124191.

[88] M. Szechyńska-Hebda, R.Z. Ghalami, M. Kamran, F. Van Breusegem, S. Karpiński, To be or not to be? Are reactive oxygen species, antioxidants, and stress signalling universal determinants of life or death? Cells 11 (2022) 4105.